Coatings **2014**, *4*, 587-601; doi:10.3390/coatings4030587

OPEN ACCESS

coatings

ISSN 2079-6412

www.mdpi.com/journal/coatings

Article

Tuning the Photocatalytic Activity of Anatase TiO_2 Thin Films by Modifying the Preferred <001> Grain Orientation with Reactive DC Magnetron Sputtering

B. Stefanov and L. Österlund *

Department of Engineering Sciences, The Ångström Laboratory, Uppsala University, P.O. Box 534, SE-75121 Uppsala, Sweden; E-Mail: bozhidar.stefanov@angstrom.uu.se

***** Author to whom correspondence should be addressed; E-Mail: lars.osterlund@angstrom.uu.se

Received: 6 June 2014; in revised form: 10 July 2014 / Accepted: 31 July 2014 / Published: 8 August 2014

Abstract: Anatase TiO_2 thin films were deposited by DC reactive magnetron sputtering on glass substrates at 20 mTorr pressure in a flow of an Ar and O_2 gas mixture. The O_2 partial pressure (P_{O_2}) was varied from 0.65 mTorr to 1.3 mTorr to obtain two sets of films with different stoichiometry. The structure and morphology of the films were characterized by secondary electron microscopy, atomic force microscopy, and grazing-angle X-ray diffraction complemented by Rietveld refinement. The as-deposited films were amorphous. Post-annealing in air for 1 h at 500 °C resulted in polycrystalline anatase film structures with mean grain size of 24.2 nm (P_{O_2} = 0.65 mTorr) and 22.1 nm (P_{O_2} = 1.3 mTorr), respectively. The films sputtered at higher O_2 pressure showed a preferential orientation in the <001> direction, which was associated with particle surfaces exposing highly reactive {001} facets. Films sputtered at lower O_2 pressure exhibited no, or very little, preferential grain orientation, and were associated with random distribution of particles exposing mainly the thermodynamically favorable {101} surfaces. Photocatalytic degradation measurements using methylene blue dye showed that <001> oriented films exhibited approximately 30% higher reactivity. The measured intensity dependence of the degradation rate revealed that the UV-independent rate constant was 64% higher for the <001> oriented film compared to randomly oriented films. The reaction order was also found to be higher for <001> films compared to randomly oriented films, suggesting that the <001> oriented film exposes more reactive surface sites.

Keywords: TiO_2; photocatalysis; DC magnetron sputtering; preferred orientation; (001) facets

1. Introduction

Photocatalytic and superhydrophillic thin films of anatase TiO_2 have attracted large research interest since the early 1970s and find application as self-cleaning, anti-fogging and anti-bacterial coatings [1–5]. Due to their intrinsic beneficial physical properties, TiO_2 films are suitable for architectural coatings, and commercially available self-cleaning glasses, tiles, cement, porcelain based on TiO_2 already exist [6–8].

There are a number of ways to deposit TiO_2 onto a glass substrate, including chemical methods such as dip-coating using sol-gel techniques [9], spray-pyrolysis [10], and atomic layer deposition [11]. Physical deposition techniques such as magnetron sputtering are industrial up-scalable technologies which allow for fast and controlled deposition of films with good optical and mechanical properties [12]. An added possibility for DC magnetron sputtering deposition of anatase TiO_2 is that the film textured can be controlled, and preferred orientated film growth in the <004> direction has been reported with improved photocatalytic properties [13].

Typically, the surfaces of TiO_2 nanocrystals are dominated by the stable {101} facets, with only a small amount of {001} facets, leading to a truncated bipyramidal shape [14,15]. The {001} facets have two times higher surface energy than {101} facets, but is expected to exhibit higher reactivity [16]. Ab initio calculations show that water dissociates on the (001) surface, while it only adsorbs molecularly on the (101) [17]. Altering the preparation conditions it was found that TiO_2 nanoparticles made by solvothermal synthesis can be prepared with altered <001>/<101> facet ratio [18–20]. In several studies it was reported that this led to an improved photocatalytic activity for the degradation of a number of liquid and gas-phase contaminants [21–23]. There are much fewer studies on sputter deposited TiO_2 films. It has been reported that sputtered TiO_2 films on biased substrates alter the texturing and preferred orientation depending on bias voltage, leading to an improved photodegradation rate of acetaldehyde as a function of increasing orientation [24]. Other reports show that changing total pressure [25], and O_2 partial pressure [26] may also affect film growth and preferential orientation of anatase films.

In the present study, we present results on the effect of preferred crystal grain orientation on the photocatalytic reactivity of anatase TiO_2 films prepared by DC magnetron sputtering. The preferred grain orientation is shown to be related to the partial pressure of O_2 in the reaction chamber. The effect of orientation on their photocatalytic properties was investigated. Both the apparent rate constant and intensity dependence of the photo-oxidation of methylene blue dye in liquid phase was studied. Our results show that even though the apparent reaction rate of the oriented films is higher, the increase in orientation does not affect the intensity dependence of the photo-degradation rate.

2. Experimental

2.1. Deposition of TiO_2 Anatase Thin Films

Anatase TiO_2 thin films were deposited by reactive DC magnetron sputtering on microscope slides glass substrates (Thermo Fischer Scientific, Waltham, MA, USA) using a Balzers UTT400 sputter system [27]. Two 5 cm diameter Ti targets (99.99% purity, Plasmaterials, Livermore, CA, USA) were used for deposition, and positioned 13 cm from the center of the sample holder, which was rotated at

approximately 3 rpm, as described elsewhere [28]. Ar and O_2 gases (both with 99.997% purity) were supplied using mass flow controllers. The Ar flow rate was set to 60 mL·min^{-1} and the total pressure in the chamber was adjusted to 20 mTorr, and kept constant in the experiment, yielding approximately the same kinetic energy of the ions impinging on the substrate and thus facilitate inter-comparisons between fabrication conditions. The O_2 flow rate was varied in the experiments and two flow rates were employed, 2 mL·min^{-1} and 4 mL·min^{-1}, respectively, corresponding to an O_2 partial pressure of P_{O_2} = 0.65 mTorr and P_{O_2} = 1.3 mTorr in the sputtering chamber. One extra sample was deposited at intermediate O_2 pressure P_{O_2} = 0.95 mTorr (3 mL·min^{-1}) to confirm the dependence of physical properties on P_{O_2} (see Table 1), but this film was not studied further here. The plasma was created by a DC power supply set to constant current mode at 0.75 A yielding 212 W direct power at P_{O_2} = 0.65 mTorr O_2, and 245 W at P_{O_2} =1.3 mTorr O_2.

At each O_2 partial pressures a total of 5 samples were sputtered. One sample with a size of 25 mm × 25 mm for X-ray diffraction measurements, and two batches consisting of two samples each deposited on larger substrates (50 mm × 25 mm, covered with a mask, thus limiting the coated area to 45 mm × 20 mm, or 900 mm^2) for the photo-catalytic experiments. Both sets of films were deposited for 35 min resulting in film thicknesses of 574 and 664 nm for the films sputtered at P_{O_2} = 0.65 and 1.3 mTorr O_2, respectively, as determined by surface profilometry (Bruker DektrakXT, Karlsruhe, Germany). The slight increase in sputtering rate from 16.4 to 19 nm·min^{-1} is likely to be due to the higher sputtering power obtained at 1.3 mTorr. The as-deposited samples were amorphous. To transform them into polycrystalline anatase they were calcined for 1 h at 500 °C. The temperature was ramped at 5 °C·min^{-1} and the samples were left to cool overnight.

2.2. Structural and Morphological Characterization

The film structure was investigated by grazing-incidence X-ray diffraction (GIXRD) employing a Siemens D5000 diffractometer equipped with parallel-beam optics and 0.4° Soller-slit collimator (Bruker AXS, Karlsruhe, Germany). The grazing angle was set to 0.5° and the diffractograms were collected with 5 s integration time and 0.05° resolution.

The film morphology was measured with scanning electron microscopy (SEM) using a FEI/Philips XL-30 environmental SEM microscope equipped with a field-emission gun (FEI, Hillsboro, OR, USA), and operated in Hi-Vac mode at 10 kV accelerating voltage.

The surface morphology was measured with atomic force microscopy (AFM) using a PSIA XE150 SPM/AFM (Park Systems Corp., Suwon, Korea) operating in non-contact mode in air at room temperature. Silicon ACTA cantilevers (AppNano, Mountain View, CA, USA) with 30 nm thick Al coating were used. The tip radius reported by the manufacturer was between 6 and 10 nm. Images were obtained at 1 Hz scanning rate over an area of 1000 nm × 1000 nm with a resolution of 256 pixels × 256 pixels.

2.3. Optical Measurements

Spectrophotometry using a Perkin-Elmer Lambda 900 spectrophotometer equipped with a 150 mm $BaSO_4$ coated integrating sphere was employed to optically determine the optical constant and film porosity. Transmission and reflectance spectra were recorded between 300 and 800 nm.

2.4. Photocatalytic Measurements

Photodegradation experiments of methylene blue (MB) dye in solution were used to quantify the photocatalytic activity of the two TiO_2 thin films with different preferred grain orientation. They will be referred to as sample "<101>" corresponding to the sample with 2% <001> orientation (*i.e.*, almost randomly oriented grains dominated by <101> facets), and sample "<001>" with 25% <001> orientation. The experiments with MB were performed in a liquid-phase reactor employing in situ laser colorimetry for chemical analysis of the MB concentration employing a λ = 365 nm diode laser, as described in detail elsewhere [29]. A standard 4 W UV tube (λ = 365 nm) was used as a light source, positioned above the sample and attached on a stand, allowing for the distance between the tube and the reaction cell to be changed, as well as the illumination intensity. The intensity of the UV tube measured with a calibrated thermopile detector (Ophir, North Andover, MA, USA) was 2.44 mW cm^{-2} at the UV tube's wall. Using the linear-source spherical emission (LSSE) model, the intensity distributions at the position of the film in the reactor was estimated to be 0.38 mW cm^{-2}.

Samples were placed on a sample holder at the bottom of the reaction cell, which was filled with 100 mL of distilled water and circulated with a magnetic stirrer. Background absorption in the reactor was measured, and then 1 mL of 100 ppm MB stock solution was added, leading to an initial concentration of 0.99 ppm. The system was allowed to reach equilibrium during a time period of 40 min allowing adsorption-desorption equilibrium between reactor walls and sample to be obtained. The MB concentration was measured in situ every 2 min during this equilibration and the increase of the laser signal at λ = 365 nm (due to MB adsorption in the reactor) was used to determine that equilibration was reached.

3. Results and Discussions

3.1. Film Structure and Morphology

It is evident from the diffractograms shown in Figure 1a that the as deposited films are completely amorphous. In contrast the heat-treated films consist only of anatase phase (Figure 1b). The different ratio between the <101> and <004> peaks in the two samples (<004> is here referred to as the <001> direction using conventional Miller indexing) suggests that they are textured and have different preferential orientation. To gain further insight, the diffractograms were Rietveld refined [30] using the PowderCell package [31] and compared with anatase crystallographic files [32]. The preferential orientation was approximated with the March-Dollase model [33], as implemented in PowderCell. This model is appropriate for films sputtered under rotation because it implies a cylindrical texturing symmetry. Rietveld refinement showed that the films consisted of polycrystalline anatase grains with mean crystallite size of 24.2 nm at P_{O_2} = 0.65 mTorr, and 22.1 nm at P_{O_2} = 1.3 mTorr. The <004> March-Dollase (MD) parameter was found to be 0.966 in the former case (R_p = 5.9, R_{exp} = 3.49) and 0.637 in the latter (R_p = 5.7, R_{exp} = 2.94). Using the Zolotoyabko equation [34], the MD parameters were converted into percentages of preferred orientation, viz.

$$\eta_{\langle hkl\rangle} = \frac{\left(1-r_{\langle hkl\rangle}\right)^3}{\left(1-r_{\langle hkl\rangle}{}^3\right)} \cdot 100\% \quad (1)$$

where $\eta_{<hkl>}$ is the degree of preferential orientation in the <*hkl*> direction in % and $r_{<hkl>}$ is the MD parameter calculated for this direction. The results from this analysis showed 2% preferential <001> orientation for the film sputtered at P_{O_2} = 0.65 mTorr, while 25% preferential orientation was found for the film sputtered P_{O_2} =1.3 mTorr. The 2% oriented film thus corresponds to almost randomly oriented grains, yielding a stronger <101> peak, due to the high relative abundance of these crystal planes in the equilibrium anatase structure. Since the measurements were done at a grazing angle of 0.5 ° only the topmost 165 nm of the films are penetrated (and the information depth is even less). Thus, we can safely assume that the structure of the surface structure is consistent with the results from the GIXRD measurements. Considering a mean crystallite size of approximately 20 nm this implies that only a thin layer corresponding to 8 "particle layers" are probed. Below we refer to the sample sputtered at P_{O_2} = 0.65 mTorr to the <101> sample, and the one sputtered at P_{O_2} =1.3 mTorr to the <001> sample.

Qualitative comparison of the Ti Kα and O Kα peaks ratio from EDX showed that the heat treated samples have the same stoichiometry. For each partial O_2 pressure the ratio between the Ti and O peak was approximately constant at 0.65, confirming that the calcination in air oxidizes the substoichiometric films to an equilibrium structure (Table 1). Corresponding data for as-deposited films showed varying results due to bleaching (indicating gradual re-oxidation) of the films in the course of EDX analysis.

The SEM images shown in Figure 2 show that the films are composed of densely packed spherically shaped particles. No significant difference was observed between the two sets of films prepared at different O_2 pressures. Cross section images were obtained at 30 ° tilting angle and showed a dense film structure with no evidence of columnar growth.

Figure 1. XRD diffractograms of post-annealed (**a**) non-oriented and (**b**) <001> oriented films (the intensity ordinates for the two samples are shifted and given in arbitrary units). Photographs of the corresponding as-deposited films are shown on as insets on the right.

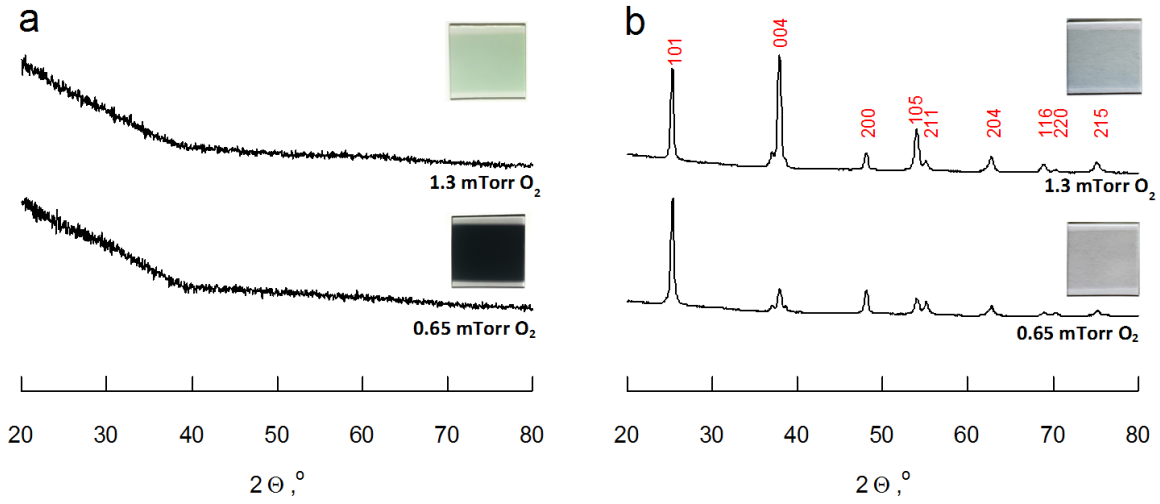

Figure 2. Scanning electron microscope micrographs showing top-view and cross sections (taken at 30 °angle of incidence) of the post-annealed films sputtered at (**a**,**c**) P_{O_2} = 0.65 mTorr, and (**b**,**d**) P_{O_2} = 1.3 mTorr.

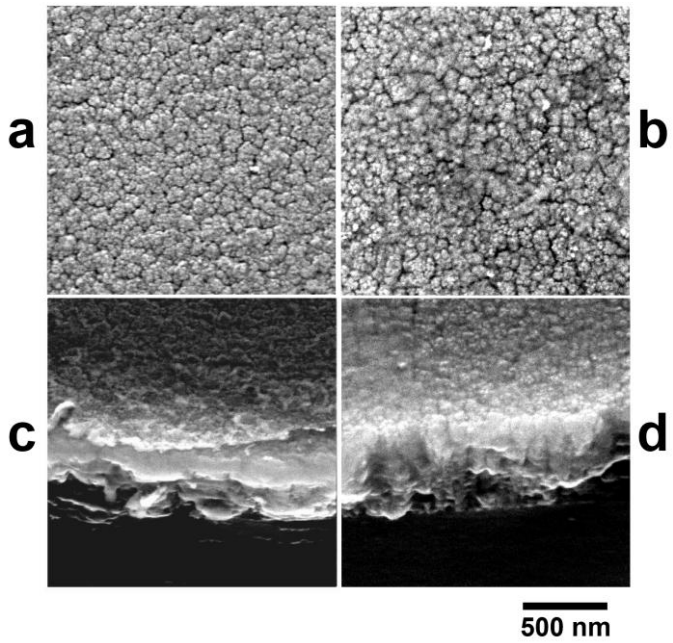

It is apparent from the AFM images (Figure 3) that the surface morphology appears similar to the results from SEM. The raw data was treated to correct for *Z*-scanner error in the *Y* direction and exported as numerical values for statistical treatment in the *R* environment [35] using homemade scripts. Two surface morphology parameters were calculated: the root mean square (rms) surface roughness, R_q, and the average surface roughness wavelength, λ_q, where the latter is defined as

$$\lambda_q = 2\pi \frac{R_q}{\Delta_q} \tag{2}$$

where Δ_q is the rms surface slope, defined as

$$\Delta_q = \sqrt{\frac{1}{N-1}\sum_{N-1}\left(\frac{\Delta Z}{\Delta x}\right)^2} \tag{3}$$

where ΔZ is the change in height for every tip movement; Δx, in the *x* direction. The data for both R_q, Δ_q and λ_q were averaged for each of the 256 scan lines, then over the trace and retrace images, and then for three different measurements at random positions over the sample surface. Typical images for both films are shown in Figure 3. The rms surface roughness was estimated to be R_q = 1.31 ± 0.04 nm and 1.41 ± 0.04 nm, respectively, for the films sputtered at P_{O_2} = 0.65 and 1.3 mTorr. The Δ_q values were determined to be Δ_q = 0.105 ± 0.003 nm and 0.123 ± 0.004 nm, respectively, which yielded an average surface wavelength of λ_q = 77.9 ± 4.03 and 73.9 ± 3.72 for films prepared at P_{O_2} = 0.65 and 1.3 mTorr, respectively. Based on these results we can conclude that the films are smooth and are similar for the two sets of films, with slightly larger surface roughness and surface roughness wavelength for the preferentially <001> oriented films (within 8%). The physical properties of the anatase TiO_2 thin films are compiled in Table 1.

Figure 3. Atomic force microscopy (AFM) micrographs for the films with (**a**) 2% and (**b**) 25% <001> orientation.

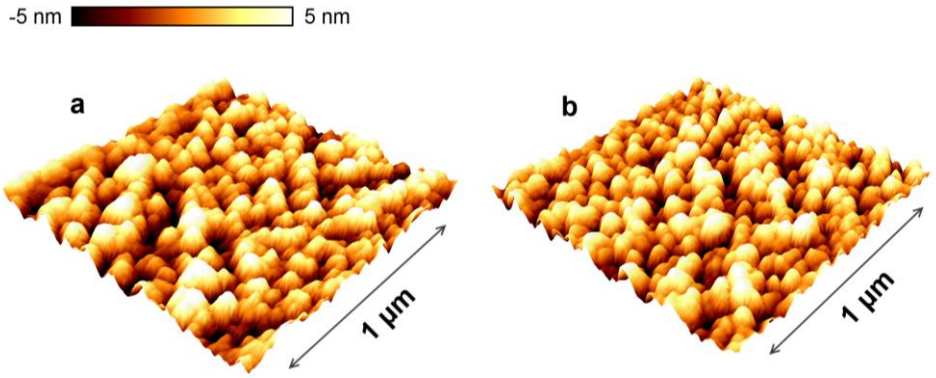

Table 1. Thin film deposition parameters and their effect on the physical properties of three samples deposited at similar conditions, but at different partial O_2 pressure, P_{O_2}.

Deposition parameters and physical properties	P_{O_2} **= 0.65 mTorr**	P_{O_2} **= 0.95 mTorr**	P_{O_2} **= 1.30 mTorr**
Total pressure (mTorr)		20	
Total flow (mL ·min^{-1})	62	63	64
O_2 flow (mL ·min^{-1})	2	3	4
Ar flow, (mL ·min^{-1})	60	60	60
Sputtering power (W)	212	224	245
Sputtering rate (nm ·min^{-1})	16	17	19
Stoichiometry of post-annealed films (from EDX, expressed as $I_{O\ K\alpha}/I_{Ti\ K\alpha}$)	0.652	0.650	0.645
Morphology			
Thickness, *d* (nm)	574	579	664
AFM rms roughness (nm)	1.3	1.1	1.4
Crystallographic properties			
March-Dollase (MD) parameter	0.966	0.810	0.637
Preferential <004> orientation, %	2	12	25
Mean crystalline size (nm)	24.2	26	22.1
Optical properties			
Refractive index, *n*	2.23	2.15	2.04
Packing density (Pullker), %	88	84	79
Optical bandgap, E_g (eV)	3.32	3.29	3.29

3.2. Optical Measurements

Spectrophotometry was employed to determine the optical constants and film porosity. The corresponding transmittances at 500 nm were measured to be 74% and 41%, respectively, for the as-deposited films, with the lower value for the films prepared at low P_{O_2}, which appear dark, almost black (Figure 1a, inset). After calcination the reflectance increased to about 70%–80% for all films, and they all became transparent with a slight visible tint due to light interference.

The optical constants and thicknesses of the two sets were determined using the envelope method suggested by Swanepoel [36]. The maxima and minima of the interference fringes at the transmittance

spectrum were fitted with a set of spline functions, enveloping the spectrum, as depicted in Figure 4. The refractive index was then calculated using Equation (4).

$$n = \left[N + \left(N^2 - s^2 \right)^{1/2} \right]^{1/2} \tag{4}$$

where s is the refractive index of the substrate and N is defined as

$$N = 2s \frac{T_M - T_m}{T_M T_m} + \frac{s^2 + 1}{2} \tag{5}$$

where T_M and T_m are the maximum and minimum of the transmittance at a given wavelength. The refractive index of the substrate was calculated using

$$s = \frac{1}{T} + \left(\frac{1}{T} - 1 \right)^{1/2} \tag{6}$$

where T is the transmittance measured at a given wavelength. For our glass substrates s was determined to be s = 1.39. The refractive indices were determined from the averaged refractive index over all visible maxima and minima, expect the ones near the bandgap, where the transmittance starts to decrease, and the error becomes larger. The average refractive indices for films sputtered at P_{O_2} = 0.65 and P_{O_2} = 1.3 mTorr obtained in this manner were determined to be n = 2.23 and n = 2.04, respectively, and did not vary much over the wavelength region depicted in Figure 4. Hence, the reported values of n were determined as an average of the positions marked with a dashed line in Figure 4.

Figure 4. Transmittance spectra for a (**a**) non-oriented film, and (**b**) <001> oriented film. Positions of maxima and minima of T used in the analysis of the optical data, as well as average T over the visible wavelength region, are denoted by dashed lines.

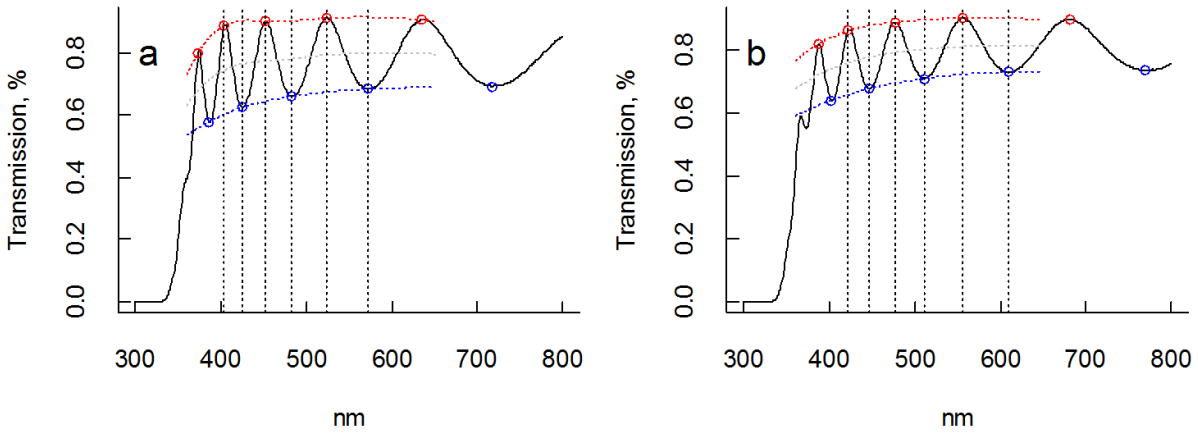

The thickness of the samples was determined using Equation (7):

$$d = \frac{\lambda_m \lambda_{m+1}}{2\left(\lambda_m \lambda_{m+1} - \lambda_{m+1} n_m \right)} \tag{7}$$

where λ_m, λ_{m+1} and n_m, n_{m+1} are the wavelength and the corresponding refractive index calculated by means of Equation (4) for any consecutive pair of maxima or minima in the UV-Vis transmittance spectra. The thicknesses calculated by means of Equation (7) were calculated to be d = 591 and 739 nm, respectively, for P_{O_2} = 0.65 and 1.3 mTorr, in good agreement with the results obtained from profilometry.

Changes in the refractive index are most likely to be associated with changes in sample porosity due different deposition conditions. The packing densities, ρ, of the two samples were therefore estimated using the Pulker equation [37].

$$\rho = \frac{\rho_f}{\rho_b} = \frac{n_f^2 - 1}{n_f^2 + 2} \cdot \frac{n_b^2 + 2}{n_b^2 - 1} \tag{8}$$

where ρ is the packing density of the sample; ρ_f and ρ_b the film and the bulk density of the material; and n_f and n_b the sample and bulk refractive index, respectively. The packing densities, corresponding to the measured refractive indices were determined to be 0.88 and 0.79, respectively, for the samples sputtered at P_{O_2} = 0.65 and 1.3 mTorr, respectively, which corresponds to a difference in porosity of about 10%, *i.e.*, a slightly increasing porosity with larger P_{O_2}, *i.e.*, a similar trend as for the surface roughness.

The optical bandgap, E_g, of the two films were calculated from the special absorption according to Hong *et al.* [38]

$$\alpha = \frac{1}{d} \ln\left(\frac{1-R}{T}\right) \tag{9}$$

where d is the thickness, T is the transmittance and, R the reflectance.

Since anatase TiO_2 is an indirect bandgap semiconductor, a plot of $\sqrt{\alpha E}$ as a function of photon energy, $E = h\nu$, should yield a linear dependence assuming parabolic band dispersion. This is a good approximation close to E_g ($E > E_g$). A linear region is discerned for both films in the region ~3.4 to ~3.6 eV, and extrapolation yields $E_g \approx 3.3$ eV for both samples in fair agreement with tabulated data of bulk anatase TiO_2 (E_g = 3.2 eV). Corresponding Tauc plots of $\sqrt{\alpha E}$ versus E are shown in Figure 5.

Figure 5. Tauc plots of $\sqrt{\alpha E}$ *vs.* photon energy, E, and least square linear fit of data for films with (**a**) no orientation and (**b**) preferential <001> orientation. In both cases the optical bandgap was estimated to be 3.3 eV.

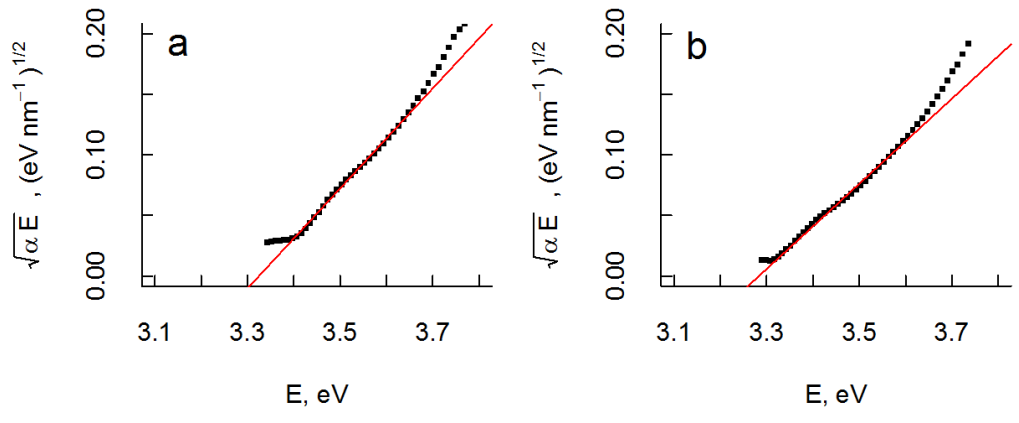

3.3. Photocatalytic Properties

Figure 6a,b show the results of the photocatalytic measurements. From the adsorption isotherms thus obtained the MB saturation coverage was determined, and found to be $8.17 \pm 0.6 \times 10^{-3}$ μmol cm^{-2} for the <101> sample and $8.29 \pm 0.8 \times 10^{-3}$ μmol cm^{-2} for the <001> sample, *i.e.*, an increase of 1.5% for the latter film. This is much smaller than the 10% increase in porosity inferred from analysis of the optical data described in Section 2.3, suggesting that the difference in porosity is related to pores inside the film structure which are inaccessible for the MB adsorption. Control experiments in a reactor containing uncoated glass substrates show that MB adsorption on reactor surfaces, other than TiO_2 film, is about 12% of the initial concentration.

After MB equilibration the UV lamp was switched on and the photodegradation of MB was measured by the increasing colometric signal. The photodegradation of MB was modeled as a pseudo-first order reaction with the apparent rate k', viz.:

$$\frac{dC}{dt} = -k't \tag{10}$$

or

$$-\ln\frac{C}{C_0} = k't \tag{11}$$

where C_0 is the initial concentration of MB (after 40 min equilibration); C is the concentration at time t. Figure 6b shows a plot of Equation (11) for a <101> and a <001> film. The apparent rate constants averaged over a set of four samples from each batch were determined to be $k'_{<101>} = 0.99 \pm 0.09 \times 10^{-3}$ min^{-1} and $k'_{<001>} = 1.29 \pm 0.17 \times 10^{-3}$ min^{-1}, corresponding to an increase of k' by approximately 30% for the preferentially <001> oriented films compared to randomly oriented films.

Figure 6. (**a**) Adsorption of methylene blue dye as a function of time, and (**b**) semi-logarithmic plot of the normalized MB concentration, C, as a function of UV irradiation time over <001> and <101> TiO_2 films. The gray line denotes the amount of dye adsorbed by reaction cell walls and uncoated glass slide in blank experiments.

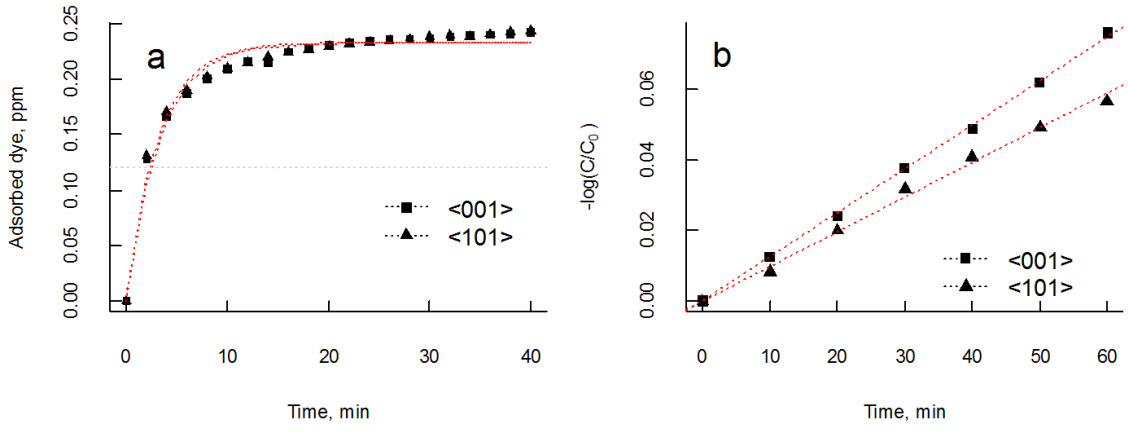

The effect of UV intensity on the photocatalytic rate for the two sets of films was investigated. Repeated experiments were performed where the distance between the sample and the UV light source was systematically varied. It was changed from 8.5 cm, which is the closest distance, limited by the

height of the reaction cell, up to 13.5 cm, 18.5 cm and 23.5 cm, yielding UV intensities at the sample position of 0.382 mW cm^{-2}, 0.158 mW cm^{-2}, 0.085 mW cm^{-2} and 0.053 mW cm^{-2}, respectively. The dependence of the rate constant of the UV light intensity was fitted using Equation (12):

$$k = k''I^{\alpha} \quad (12)$$

where k'' is the intensity independent rate constant, k is the apparent rate constant, I is the UV light intensity, and α is the reaction order by light intensity.

Figure 7 shows the effect of UV intensity on the photodegradation rate with different degree of preferential <001> orientation. In each case the experiments were conducted using four different samples. It was found that the increased orientation changes the way the catalyst is affected by the intensity of UV light. The less-oriented sample <101> showed an almost UV intensity independent rate constant for MB photodegradation with a rate constant $k''_{<101>} = 1.19 \times 10^{-3}$ min^{-1} and reaction order of α = 0.18. In contrast the <001> sample yielded a rate constant of $k''_{<001>} = 1.95 \times 10^{-3}$ min^{-1} and a reaction order of α = 0.42. Thus the UV independent rate constant k'' is 64% larger for the <001> oriented film. Again, this cannot be accounted for by a larger exposed surface area (higher porosity of surface roughness) as shown by the microscopy data, the estimates of film porosity, and surface coverage of MB. Instead it must be attributed to an intrinsic higher reactivity for the preferentially <001> oriented films. Mills and coworkers have reported that for thick, porous catalysts the rate constant, the intensity dependence can be divided into three regions [39]. The first region, at very low intensities, where the rate increases linearly with light intensity; a second region, at medium light intensities, where a square root dependence is observed, and a third region, at high intensities, where photon flux no longer limits the photo-degradation rate, and rate becomes independent of further increase of the light intensity. We can conclude from our measurements that for the randomly oriented grains dominated by {101} surfaces, the photo-degradation rate is not limited by UV intensity (with an almost constant rate as a function of UV intensity, α = 0.18). Given that our films are thin and non-porous with undeveloped surface (based on the AFM measurements) we assign this to a small number of reactive sites and/or exposure of reactive sites with low reactivity. In contrast, for the preferentially <001> oriented films, we find α = 0.42, which suggests that these films have a larger number of reactive sites and/or expose a larger fraction of more reactive sites (Table 2).

Figure 7. Methylene blue photo-degradation rate as a function of UV intensity for (**a**) a randomly oriented (<101>) TiO_2 film, and (**b**) a preferentially <001> orientated TiO_2 film. The dashed line is a guide to the eye.

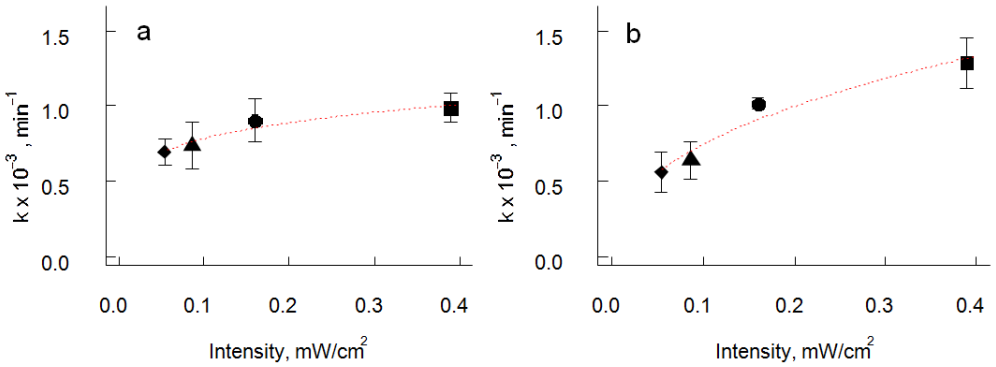

Furthermore, the UV intensity independent rate constant points to a total increase of activity by 61%. This is a dramatic increase, keeping in mind that the XRD analysis points to only 25% of the crystallites, oriented in the <001> direction (which does not directly translate to 25% increase of surface {001} coverage). For comparison, Yang *et al*. [40] demonstrated a novel synthesis of colloidal catalyst with 70% exposed highly-reactive {100} facets. Compared to Degussa P25 it showed 3-fold increase in the photo-oxidation rate of MB, which is similar to our results.

Table 2. Kinetic parameters for the photocatalytic degradation of MB for the samples with <001> preferential orientation, and with dominant <101> orientation (randomly oriented grains).

Samples	Orientation	
	<101> (random)	**<001>**
Apparent rate constant, $k'_{<hkl>}$ ($\times 10^{-3}$ min^{-1})	0.986 ± 0.09	1.286 ± 0.17
Intensity independent rate constant, $k''_{<hkl>}$ ($\times 10^{-3}$ min^{-1})	1.19	1.95
UV intensity reaction order, a	0.18	0.42

4. Conclusions

We have demonstrated that by purposefully adjusting the partial oxygen pressure in the sputtering chamber, reactive DC magnetron sputtering can be used to control the amount of preferential <001> orientation in TiO_2 thin films. The increased orientation was shown to lead to increased photocatalytic activity, which was attributed to exposure of a larger fraction of exposed reactive {001} facets at the film surface. The films with higher orientation also responded more strongly to changes in the intensity, yielding a significantly higher (64%) UV-independent photodegradation rate constant. Moreover, the reaction order was found to be almost independent of intensity for the <101> films (α = 0.18), while it was α = 0.42 for the preferentially oriented <001> films, suggesting that the preferentially <001> oriented films expose more reactive sites.

Acknowledgements

This work was funded by the European Research Council under the European Community's Seventh Framework Program (FP7/2007-2013)/ERC Grant Agreement No. 267234 ("GRINDOOR").

Author Contributions

Bozhidar Stefanov carried out all experiments, performed the data analysis and wrote the original manuscript. Lars Österlund conceived the idea, designed the structure of article and revised the manuscript.

Conflicts of Interest

The authors declare no conflict of interest.

References

1. Paz, Y.; Luo, Z.; Rabenberg, L.; Heller, A.J. Photooxidative self-cleaning transparent titanium-dioxide films on glass. *Mater. Research. Soc.* **1995**, *10*, 2842–2848.
2. Mellott, N.P.; Durucan, C.; Pantano, C.G.; Guglielmi, M. Commercial and laboratory prepared titanium dioxide thin films for self-cleaning glasses: Photocatalytic performance and chemical durability. *Thin Solid Films* **2006**, *502*, 112–120.
3. Ganesh, V.A.; Raut, H.K.; Nair, A.S.; Ramakrishna, S. A review on self-cleaning coatings. *J. Mater. Chem.* **2011**, *21*, 16304–16322.
4. Evans, P.; Sheel, D.W. Photoactive and antibacterial TiO_2 thin films on stainless steel. *Surf. Coat. Technol.* **2007**, *201*, 9319–9324.
5. Fu, G.; Vary, P.S.; Lin, C.-T. Anatase TiO_2 nanocomposites for antimicrobial coatings. *J. Phys. Chem. B.* **2005**, 109, 8889–8898.
6. Parkin, I.P.; Palgrave, R.G. Self-cleaning coatings. *J. Mater. Chem.* **2005**, *15*, 1689–1695.
7. Mills, A.; Lepre, A.; Elliott, N.; Bhopal, S.; Parkin, I.P.; O'Neill, S.A. Characterisation of the photocatalyst Pilkington Activ (TM): A reference film photocatalyst? *J. Photochem. Photobiol. A.* **2003**, *160*, 213–224.
8. Guo, S.; Wu, Z.-B.; Zhao, W.-R. TiO_2-based building materials: Above and beyond traditional applications. *Chin. Sci. Bull.* **2009**, *54*, 1137–1142.
9. Matsuda, A.; Kotani, Y.; Kogure, T.; Tatsumisago, M.; Minami, T. Transparent anatase nanocomposite films by the sol-gel process at low temperatures. *J. Am. Ceram. Soc.* **2000**, *83*, 229–239.
10. Abou-Helal, M.O.; Seeber, W.T. Preparation of TiO_2 thin films by spray pyrolysis to be used as a photocatalyst. *App. Surf. Sci.* **2002**, *195*, 53–62.
11. Liu, G.X.; Shan, F.K.; Lee, W.J.; Lee, G.H.; Kim, I.S.; Shin, B.C.; Yoon, S.G.; Cho, C.R. Transparent titanium dioxide thin film deposited by plasma-enhanced atomic layer deposition. *Integrat. Ferroelectr.* **2006**, *81*, 239–248.
12. Haseeb, A.S.M.A.; Hasan, M.M.; Masjuki, H.H. Structural and mechanical properties of nanostructured TiO_2 thin films deposited by RF sputtering. *Surf. Coat. Technol.* **2010**, *205*, 338–344.
13. Howitt, D.G.; Harker, A.B. The oriented growth of anatase in thin films of amorphous titania. *J. Mater. Res.* **1987**, *2*, 201–210.
14. Diebold, U.; Ruzycki, N.; Herman, G.; Selloni, A. One step towards bridging the materials gap: Surface studies of TiO_2 anatase. *Catal. Today* **2003**, *85*, 93–100.
15. Lazzeri, M.; Vittadini, A.; Selloni, A. Structure and energetics of stoichiometric TiO_2 anatase surfaces. *Phys. Rev. B.* **2001**, *63*, doi:10.1103/PhysRevB.63.155409.
16. Gong, X.; Selloni, A. Reactivity of anatase TiO_2 nanoparticles: The role of the minority (001) surface. *J. Phys. Chem. B* **2005**, *109*, 19560–19562.
17. Vittadini, A.; Selloni, A.; Rotzinger, F.P.; Grätzel, M. Structure and energetics of water adsorbed at TiO_2 anatase (101) and (001) surfaces. *Phys. Rev. Lett.* **1998**, *81*, 2954–2957.
18. Nguyen, C.K.; Cha, H.G.; Kang, Y.S. Axis-Oriented, Anatase TiO_2 Single Crystals with Dominant {001} and {100} Facets. *Cryst. Growth Des.* **2011**, *11*, 3947–3953.

19. Liu, B.; Aydil, E.S. Anatase TiO_2 films with reactive {001} facets on transparent conductive substrate. *Chem. Commun.* **2011**, *47*, 9507–9509.
20. Wang, L.; Zang, L.; Zhao, J.; Wang, C. Green synthesis of shape-defined anatase TiO_2 nanocrystals wholly exposed with {001} and {100} facets. *Chem. Commun.* **2012**, *48*, 11736–11738.
21. Zhang, J.; Chen, W.; Xi, J.; Ji, Z. {001} Facets of anatase TiO_2 show high photocatalytic selectivity. *Mater. Lett.* **2012**, *79*, 259–262.
22. Cao, F.-L.; Wang, J.-G.; Lv, F.-J.; Zhang, D.-Q.; Huo, Y.-N.; Li, G.-S.; Li, H.-X.; Zhu, J. Photocatalytic oxidation of toluene to benzaldehyde over anatase TiO_2 hollow spheres with exposed {001} facets. *Catal. Commun.* **2011**, *12*, 946–950.
23. Li, B.; Zhao, Z.; Gao, F.; Wang, X.; Qiu, J. Mesoporous microspheres composed of carbon-coated TiO_2 nanocrystals with exposed {001} facets for improved visible light photocatalytic activity. *App. Catal. B.* **2014**, *147*, 958–964.
24. Lyandres, O.; Finkelstein-Shapiro, D.; Chakthranont, P.M.; Graham, K.; Gray, A. Preferred Orientation in Sputtered TiO_2 Thin Films and Its Effect on the Photo-Oxidation of Acetaldehyde. *Chem. Mater.* **2012**, *24*, 3355–3362.
25. Meng, L.-J.; dos Santos, M.P. The influence of oxygen partial-pressure on the properties of dc reactive magnetron-sputtered titanium-oxide films. *Thin Solid Films* **1993**, *226*, 22–29.
26. Sério, S.; Melo Jorge, M.E.; Maneira, M.J.P.; Nunes, Y. Influence of O_2 partial pressure on the growth of nanostructured anatase phase TiO_2 thin films prepared by DC reactive magnetron sputtering. *Mat. Chem. Phys.* **2011**, *126*, 73–81.
27. Le Bellac, D.; Niklasson, G.A.; Granqvist, C.G. Angular-selective optical transmittance of anisotropic inhomogeneous Cr-based films made by sputtering. *J. Appl. Phys.* **1995**, *77*, 6145–6151.
28. Kharrazi, M.; Azens, A.; Kullman, L.; Granqvist, C.G. High-rate dual-target dc magnetron sputter deposition of electrochromic MoO_3 films. *Thin Solid Films* **1997**, *295*, 117–121.
29. Stefanov, B.I.; Kaneva, N.V.; Puma, G.L.; Dushkin, C.D. Novel integrated reactor for evaluation of activity of supported photocatalytic thin films: Case of methylene blue degradation on TiO_2 and nickel modified TiO_2 under UV and visible light. *Colloids Surf. A* **2011**, *382*, 219–225.
30. Rietveld, H.M. A profile refinement method for nuclear and magnetic structures. *J. Appl. Crystallogr.* **1969**, *2*, 65–71.
31. Kraus, W.; Nolze, G. POWDER CELL—A program for the representation and manipulation of crystal structures and calculation of the resulting X-ray powder patterns. *J. Appl. Crystallogr.* **1996**, *29*, 301–303.
32. Horn, M.; Schwerdtfeger, C.F.; Meagher, E.P. Refinement of structure of anatase at several temperatures. *Z. Krist.* **1972**, *136*, 273–281.
33. Dollase, W.A. Correction of intensities for preferred orientation in powder diffractometry—Application of the march model. *J. Appl. Crystallogr.* **1986**, *19*, 267–272.
34. Zolotoyabko, E. Determination of the degree of preferred orientation within the March-Dollase approach. *J. Appl. Crystallogr.* **2009**, *42*, 513–518.

35. *R*—A language and environment for statistical computing; R Foundation for Statistical Computing: Vienna, Austria. Available online: http://www.R-project.org/ (accessed on 9 July 2014).
36. Swanepoel, R. Determination of the thickness and optical-constants of amorphous-silicon. *J. Phys. E Sci. Instrum.* **1983**, *16*, 1214–1222.
37. Pulker, H.K. Characterization of optical thin-films. *Appl. Optic.* **1979**, *18*, 1969–1977.
38. Hong, S.; Kim, E.; Kim, D.-W.; Sung, T.-H.; No, K. On measurement of optical band gap of chromium oxide films containing both amorphous and crystalline phases. *J. Non-Cryst. Solids* **1997**, *221*, 245–254.
39. Mills, A.; Wang, J.; Ollis, D.F. Kinetics of liquid phase semiconductor photoassisted reactions: Supporting observations for a pseudo-steady-state model. *J. Phys. Chem. B* **2006**, *110*, 14386–14390.
40. Yang, Y.; Wang, G.; Deng, Q.; Kang, S.; Ng, D.H.L.; Zhao, H. A facile synthesis of single crystal TiO_2 nanorods with reactive {100} facets and their enhanced photocatalytic activity. *CrystEngComm* **2014**, *16*, 3091–3096.